The prospects for electron Bernstein wave heating of spherical tokamaks

R. A. Cairns and C. N. Lashmore-Davies

Citation: Phys. Plasmas **7**, 4126 (2000); doi: 10.1063/1.1290051
View online: http://dx.doi.org/10.1063/1.1290051
View Table of Contents: http://pop.aip.org/resource/1/PHPAEN/v7/i10
Published by the American Institute of Physics.

Related Articles

Toroidal ripple transport of beam ions in the mega-ampère spherical tokamak
Phys. Plasmas 19, 072514 (2012)

Global model of a gridded-ion thruster powered by a radiofrequency inductive coil
Phys. Plasmas 19, 073512 (2012)

Optics of ion beams for the neutral beam injection system on HL-2A Tokamak
Rev. Sci. Instrum. 83, 073307 (2012)

Initial measurements of fast ion loss in KSTAR
Rev. Sci. Instrum. 83, 10D305 (2012)

Thermo-magneto coupling in a dipole plasma
Phys. Plasmas 19, 072303 (2012)

Additional information on Phys. Plasmas

Journal Homepage: http://pop.aip.org/
Journal Information: http://pop.aip.org/about/about_the_journal
Top downloads: http://pop.aip.org/features/most_downloaded
Information for Authors: http://pop.aip.org/authors

ADVERTISEMENT

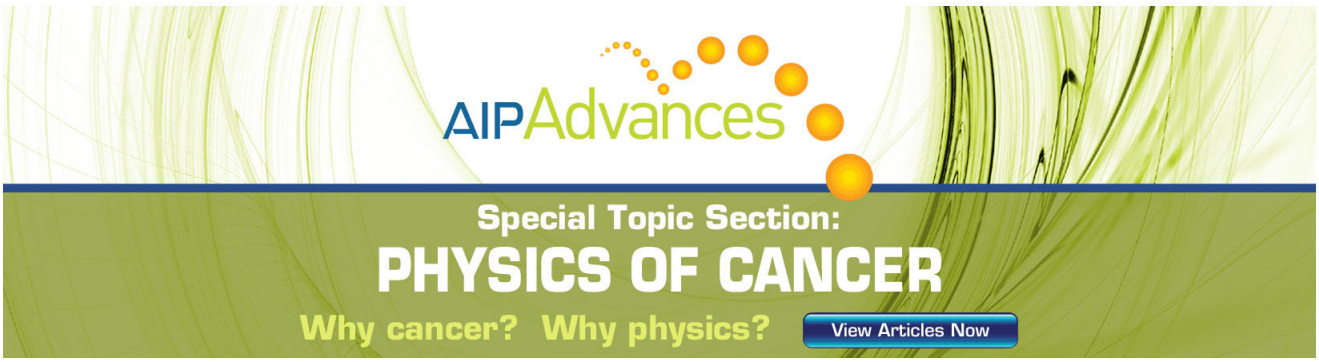

Downloaded 08 Aug 2012 to 194.81.223.66. Redistribution subject to AIP license or copyright; see http://pop.aip.org/about/rights_and_permissions

The prospects for electron Bernstein wave heating of spherical tokamaks

R. A. Cairns
School of Mathematics and Statistics, University of St Andrews, KY16 9SS, United Kingdom

C. N. Lashmore-Davies[a)]
EURATOM/UKAEA Fusion Association, Culham Science Centre, Abingdon, Oxon, OX14 3DB, United Kingdom

(Received 2 February 2000; accepted 5 July 2000)

Electron Bernstein waves are analyzed as possible candidates for heating spherical tokamaks. An inhomogeneous plane slab model of the plasma with a sheared magnetic field is used to calculate the linear conversion of the ordinary mode (O-mode) to the extraordinary mode (X-mode). A formula for the fraction of the incident O-mode energy which is converted to the X-mode at the O-mode cutoff is derived. This fraction is then able to propagate to the upper hybrid resonance where it is converted to the electron Bernstein mode. The damping of electron Bernstein waves at the fourth harmonic resonance, corresponding to a 60 GHz source on the Mega Amp Spherical Tokamak MAST [A. C. Darke *et al.*, Proceedings of the 16th Symposium on Fusion Energy, Champaign-Urbana, Illinois (IEEE, Piscataway, NJ, 1995, Vol. 2, p. 1456)], is computed. For comparison, results are also presented for a lower frequency source, close to the fundamental electron cyclotron resonance. Both the fundamental and the fourth harmonic are shown to be so strongly absorbing that the electron Bernstein wave would be totally absorbed in the outer regions of the resonance. This feature implies that electron Bernstein wave current drive (on- or off-axis) could be very efficient. [S1070-664X(00)03510-2]

I. INTRODUCTION

Spherical tokamaks present a new challenge to heating and current drive schemes because of the high-plasma densities, and low magnetic fields. The Mega Amp Spherical Tokamak (MAST[1]) will build on the success of the Small, Tight Aspect Ratio (START[2]) and employ neutral beam heating. However, since the subject of spherical tokamaks is relatively new it is desirable to test other heating schemes, such as the high harmonic fast wave heating system to be used on the National Spherical Tokamak Experiment (NSTX[3]). An alternative scheme which may be useful is electron cyclotron resonance heating, ECRH. Such a scheme is planned for MAST, since ~ 1.5 MW of radio frequency power is available with 60 GHz gyrotrons. For this reason our numerical results are obtained with MAST parameters. It is also clear that the conventional application of ECRH by relying on either the ordinary, O-mode, or extraordinary, X-mode is not very promising for spherical tokamaks for the following reasons. The harmonics which would be resonant near to the center of MAST (for a 60 GHz source) would be the third and fourth (see Fig. 1). The damping of these harmonics would be extremely weak for both the O-mode and the X-mode and so central heating (and current drive) would be difficult and probably ineffective. The second harmonic X-mode, which is strongly absorbing, would be resonant on the high field side of MAST at $r/a \approx 0.6$. Hence, heating in the outer regions would be possible but the central density would need to be less than $\sim 3\times 10^{19}$ m^{-3}, the low density X-mode cutoff.

There is, however, another possibility which might allow the 60 GHz gyrotrons to be used much more effectively. This requires that the gyrotron power be coupled to electron Bernstein waves, which also deposit their energy at harmonics of the electron cyclotron frequency. The advantages of electron Bernstein waves are that they are not subject to any density limit and (as we shall see) they are strongly absorbed at high harmonics, as well as the fundamental and low harmonics. The disadvantage is that the excitation of electron Bernstein waves, which are predominantly electrostatic, is not straightforward.

Direct coupling to electron Bernstein waves is a possibility but, because of their short wavelength, impedance matching will be required.[4] A more promising approach involves linear mode conversion from the electromagnetic X-mode to the electron Bernstein wave at the upper hybrid resonance. There are two ways of achieving this. The first requires the X-mode to tunnel through the evanescent region between the low-density R-cutoff[5] and the upper hybrid resonance. It has been shown that this process can be optimized by taking account of the high-density L-cutoff[5] and considering the propagation of the X-mode in this triplet configuration,[6] i.e., the triplet formed by the three critical surfaces, R-cutoff, upper hybrid resonance and L-cutoff. The second way utilizes the so-called Z-hole effect, first discussed with reference to ionospheric propagation.[7] This requires the O-mode to impinge on its cutoff surface, where the wave frequency ω matches the local electron plasma frequency, with $n_\parallel^2 = \Omega_e/(\omega+\Omega_e)$ where $\Omega_e \equiv |\omega_{ce}|$, $n_\parallel = ck_\parallel/\omega, k_\parallel$ is the component of the wave vector in the direction of the equilibrium magnetic field and ω_{ce} is the-

a)Electronic mail: c.n.l-d@ukaea.org.uk

Downloaded 08 Aug 2012 to 194.81.223.66. Redistribution subject to AIP license or copyright; see http://pop.aip.org/about/rights_and_permissions

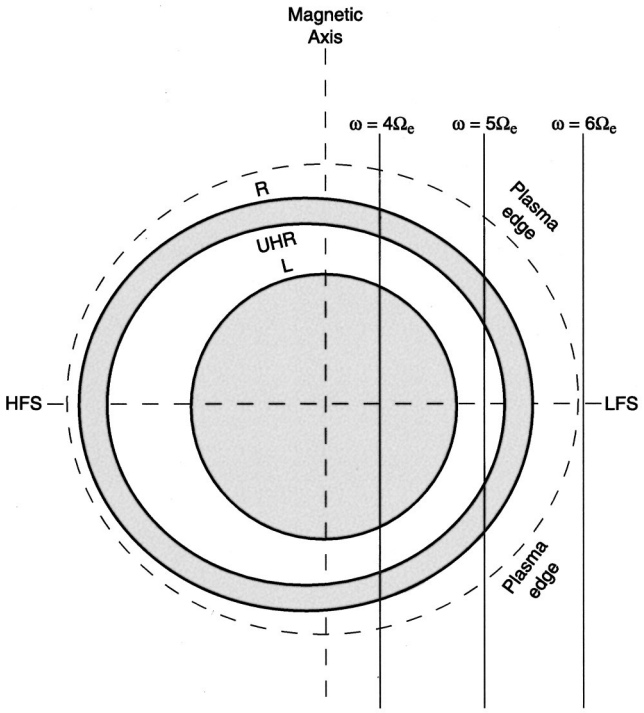

FIG. 1. Cutoff and resonance surfaces for MAST parameters ($B_0=0.63$T, $R=0.7$ m, $a=0.5$ m) and a frequency of 60 GHz. Shaded regions are nonpropagating for the X-mode.

electron cyclotron frequency including the sign of the charge. Under these conditions the O-mode cutoff is degenerate with the high density X-mode cutoff. As a result, the O-mode is totally converted to the X-mode, which is then able to propagate to lower density where it encounters the upper hybrid resonance and is, in turn, totally converted to an electron Bernstein wave. This mechanism was originally proposed for plasma heating by Preinhaelter and Kopecky.[8] It has recently been successfully demonstrated to produce heating in overdense plasmas on the W7-AS (Wendelstein-7) stellarator by Laqua *et al.*[9] and has been suggested as a possible heating scheme for NSTX by Batchelor and Bigelow.[10] The inverse process has also been proposed as a diagnostic of the electron temperature for MAST.[11]

Since electron Bernstein waves are not subject to a density limit and since they are absorbed strongly at the fundamental and all harmonics, there is a wide choice of frequencies. A proof of principle experiment will inevitably attempt to couple power to EBW's (electron Bernstein wave) at whatever frequency is locally available. However, in the longer term, overlap of adjacent harmonic resonances would be detrimental to electron Bernstein wave current drive (EBWCD) and could be a problem in a future spherical tokamak power plant. Such harmonic overlap would be minimized by working at the fundamental. Hence, in addition to the harmonic resonance corresponding to the 60 GHz source presently available to MAST, we will also consider the excitation and absorption of electron Bernstein waves in the vicinity of the fundamental frequency.

In this paper, we concentrate on the O–X–EBW conversion process and in Sec. II extend the previous calculations to include the effect of magnetic shear which can be very strong in spherical tokamaks. These calculations are carried out for $\omega\simeq 4\Omega_e$ and $\omega\simeq\Omega_e$. Section III is concerned with the damping of electron Bernstein waves in the vicinity of the fourth harmonic resonance and the fundamental resonance. A summary and conclusions are given in Sec. IV.

II. THE O–X CONVERSION

The conversion of the O-mode to the X-mode at the plasma resonance was first considered for its application to plasma heating in Ref. 8. The analysis in Ref. 8 was later generalized by Weitzner and Batchelor[12] and by Mjolhus.[13] The authors of Ref. 12 noted that after conversion the X-mode continues to propagate to higher densities until it reaches another critical point, where it is reflected; it then travels to lower density where it encounters the upper hybrid resonance. The reflection referred to in Ref. 12 does not occur at a cutoff, however, but is due to the X-mode changing from a backward wave (with group and phase velocities in opposite directions) to a forward wave.[14] There is complete reflection where the group velocity reverses and, assuming that tunneling between the upper hybrid resonance and the low-density cutoff is negligible, complete conversion to an electron Bernstein wave at the upper hybrid. This is best appreciated from a consideration of the $\omega-k_\perp$ diagram, where $k_\perp$ is the component of the wave vector perpendicular to the equilibrium magnetic field.

The cold plasma dispersion relation can be written in the form[15]

$$\varepsilon_\perp n_\perp^4-[(\varepsilon_\perp-n_\parallel^2)(\varepsilon_\perp+\varepsilon_\parallel)-\varepsilon_{xy}^2]n_\perp^2$$

$$+\varepsilon_\parallel[(\varepsilon_\perp-n_\parallel^2)^2-\varepsilon_{xy}^2]=0, \tag{1}$$

where

$$\varepsilon_\perp=1-\sum_j\frac{\omega_{pj}^2}{(\omega^2-\omega_{cj}^2)}, \tag{2}$$

$$\varepsilon_{xy}=\sum_j\frac{\omega_{pj}^2\omega_{cj}}{\omega(\omega_{cj}^2-\omega^2)}, \tag{3}$$

$$\varepsilon_\parallel=1-\sum_j\frac{\omega_{pj}^2}{\omega^2}, \tag{4}$$

and ω_{cj} is the cyclotron frequency of species j (including the sign of the charge). ω_{pj} is the plasma frequency of species j, $n_\parallel=ck_\parallel/\omega$, $n_\perp=ck_\perp/\omega$ where $k_\parallel$ is the wave number parallel to the equilibrium magnetic field and $k_\perp$ is the perpendicular wave number. Let us now obtain a solution of Eq. (1) in the vicinity of the O-mode cutoff where $\omega=\omega_{pe}$ and where $n_\perp=0$. We assume

$$\omega\simeq\omega_{pe}+\delta\omega, \tag{5}$$

$$\text{and } n_\perp\simeq\delta n_\perp. \tag{6}$$

Since we are concerned with the region near to cutoff we may neglect the $n_\perp^4$ term in Eq. (1), which is therefore, expressed in the form

Downloaded 08 Aug 2012 to 194.81.223.66. Redistribution subject to AIP license or copyright; see http://pop.aip.org/about/rights_and_permissions

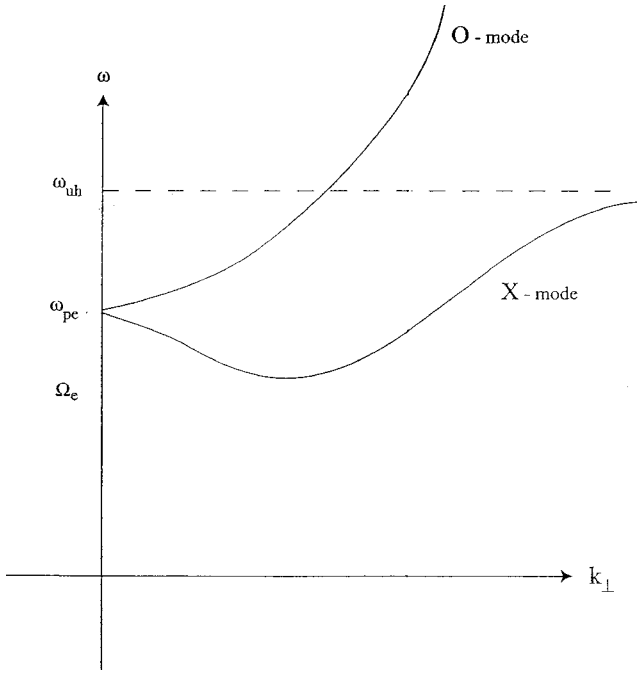

FIG. 2. Frequency (ω) vs perpendicular wave number ($k_\perp$) diagram for critical value of $k_\parallel=\omega\Omega_e/[c(\omega+\Omega_e)]$ for conversion of O-mode to X-mode.

$$-[(\varepsilon_\perp-n_\parallel^2)(\varepsilon_\perp+\varepsilon_\parallel)+\varepsilon_{xy}^2](\delta n_\perp)^2 + \left(1-\frac{\omega_{pe}^2}{\omega^2}\right)\left[1-\frac{\omega_{pe}^2}{\omega(\omega-\Omega_e)}-n_\parallel^2\right] \times\left[1-\frac{\omega_{pe}^2}{\omega(\omega+\Omega_e)}-n_\parallel^2\right]\simeq 0, \tag{7}$$

where $\Omega_e>0$. We now impose the additional constraint that

$$1-\frac{\omega_{pe}^2}{\omega(\omega+\Omega_e)}-n_\parallel^2=0, \tag{8}$$

which is the high-density cutoff condition for the X-mode. Since we have already assumed that $\omega=\omega_{pe}$, this gives a critical value for $n_\parallel$ given by

$$n_{cr}^2=\frac{\Omega_e}{(\omega_{pe}+\Omega_e)}. \tag{9}$$

Hence, substituting Eqs. (5), (6), and (9) into Eq. (7) we obtain

$$(\delta\omega)^2\simeq\frac{\omega_{pe}^2}{4}\,\frac{\Omega_e(\omega_{pe}+\Omega_e)}{(2\omega_{pe}^2+3\omega_{pe}\Omega_e+2\Omega_e^2)}(\delta n_\perp)^2. \tag{10}$$

This enables the $\omega-k_\perp$ diagram to be obtained for $k_\parallel=k_{cr}$ which is shown in Fig. 2. k_{cr} is defined by Eq. (9). It is clear that the X-mode is a backward wave in the vicinity of the degenerate cutoff at $\omega=\omega_{pe}$. However, the X-mode must eventually connect to the upper hybrid resonance and hence must pass through a minimum where $d\omega/dk_\perp=0$ and the X-mode becomes a forward wave.

Let us now analyze this process in an inhomogeneous plasma in a sheared magnetic field. We consider a plane slab model in which the direction of inhomogeneity is in the x direction. The magnetic field and the plasma density both vary with x. We suppose that the radiation reaches the surface where $\omega=\omega_{pe}$, at an angle near to the critical condition for total conversion from the O- to the X-mode. The axes may be chosen so that, at the value of x where $\omega=\omega_{pe}$, the magnetic field is in the z direction. Magnetic shear is introduced as follows. The coordinates (x,y,z) will be assumed to be fixed and oriented as above at the critical surface. An x-dependent system (x',y',z') will be oriented with the z' axis along the magnetic field. If $\theta(x)$ is the rotation angle, then

$$\begin{pmatrix}x'\\y'\\z'\end{pmatrix}=\begin{pmatrix}1&0&0\\0&\cos\theta&\sin\theta\\0&-\sin\theta&\cos\theta\end{pmatrix}\begin{pmatrix}x\\y\\z\end{pmatrix}, \tag{11}$$

and all other vector quantities are related in the same way. By definition $\theta(0)=0$, and we shall assume that in the region of interest θ is small. In this case we can take $\cos\theta\approx1$, and $\sin\theta\approx\theta$ in Eq. (11). We allow for a y component of the wave vector, but since total conversion to the X-mode only occurs for $k_y=0$, we assume that k_y is small so that we have from Eq. (11)

$$n_y'\approx n_y+\theta n_z, \qquad n_z'\approx-\theta n_y+n_z\approx n_z, \tag{12}$$

where products of small quantities are neglected. In the rotated frame the local dielectric tensor takes the usual form and if we then express primed quantities in terms of unprimed quantities, we get, to lowest order,

$$\begin{pmatrix}\varepsilon_\perp-n_z^2-n_y^2 & n_xn_y+i\varepsilon_{xy} & n_xn_z\\ n_xn_y-i\varepsilon_{xy} & \varepsilon_\perp-n_x^2-n_z^2 & n_yn_z+\theta n_z^2\\ n_xn_z & n_yn_z+\theta n_z^2 & \varepsilon_\parallel-n_x^2-n_y^2\end{pmatrix} \times\begin{pmatrix}E_x\\E_y+\theta E_z\\E_z-\theta E_y\end{pmatrix}=0. \tag{13}$$

In the vicinity of the critical surface, n_x is small so that we may again neglect terms which are quadratic in n_y and n_x. The middle line of Eq. (13) gives

$$E_y=\frac{i\varepsilon_{xy}}{(\varepsilon_\perp-n_z^2)}E_x-\frac{(n_yn_z+\varepsilon_\perp\theta)}{(\varepsilon_\perp-n_z^2)}E_z. \tag{14}$$

Using Eq. (14) and the other two lines of Eq. (13), we obtain

$$\frac{\{(\varepsilon_\perp-n_z^2)^2-\varepsilon_{xy}^2\}}{(\varepsilon_\perp-n_z^2)}E_x-\frac{i\varepsilon_{xy}(n_y+\theta n_z)}{(\varepsilon_\perp-n_z^2)}E_z+n_xn_zE_z=0, \tag{15}$$

$$n_xn_zE_x+\frac{i\varepsilon_{xy}(n_yn_z+\theta n_z^2)}{(\varepsilon_\perp-n_z^2)}E_x+\varepsilon_\parallel E_z=0, \tag{16}$$

where products of θ, n_y, n_x, and $\varepsilon_\parallel$ have all been neglected. Making the substitution, $n_x\rightarrow-id/dx$ where distance is

Downloaded 08 Aug 2012 to 194.81.223.66. Redistribution subject to AIP license or copyright; see http://pop.aip.org/about/rights_and_permissions

scaled in units of c/ω, Eqs. (15) and (16) yield a pair of differential equations for the inhomogeneous system valid in the vicinity of the surface where $\omega=\omega_{pe}$

$$\frac{dE_x}{dx}=\frac{\varepsilon_{xy}(n_y+\theta n_z)}{(\varepsilon_\perp-n_z^2)}E_x-\frac{i\varepsilon_\parallel}{n_z}E_z, \tag{17}$$

$$\frac{dE_z}{dx}=\frac{-i\{(\varepsilon_\perp-n_z^2)^2-\varepsilon_{xy}^2\}}{n_z(\varepsilon_\perp-n_z^2)}E_x-\frac{\varepsilon_{xy}(n_y+\theta n_z)}{(\varepsilon_\perp-n_z^2)}E_z. \tag{18}$$

If we take $x=0$ at the point where $\omega=\omega_{pe}$, then we have $\varepsilon_\parallel\approx -x/L_n$ with L_n a scale length associated with the density gradient. If δ is the mismatch in n_z compared to the critical value $n_{cr}=(\varepsilon_\perp+\varepsilon_{xy})^{1/2}$ at $x=0$ ($\delta=n_z-n_{cr}$), then Eqs. (17) and (18) take the following form in the critical region:

$$\frac{dE_x}{dx}=-\left(n_y+n_{cr}\frac{xc}{\omega L_\theta}\right)E_x+\frac{ixc}{n_{cr}\omega L_n}E_z, \tag{19}$$

$$\frac{dE_z}{dx}=i\left\{4\delta+\frac{2\omega xc}{\omega L_n n_{cr}(\omega+\Omega_e)}\right\}E_x+\left(n_y+n_{cr}\frac{xc}{\omega L_\theta}\right)E_z, \tag{20}$$

where the scale length of the magnetic shear has been introduced by taking $\theta\approx x/L_\theta$ near $x=0$.

Let us now follow previous work and calculate the transmission coefficient using a WKB method. Assuming a solution in the form $\exp(\pm i\int^x k(x')dx')$ in Eqs. (19) and (20), we obtain

$$k^2(x)=\alpha\left\{x^2+\left(\frac{4c\delta}{\alpha\omega L_n n_{cr}}-\frac{2cn_y n_{cr}}{\omega L_\theta\alpha}\right)x-\frac{n_y^2}{\alpha}\right\}, \tag{21}$$

where

$$\alpha=\frac{2\omega}{(\omega+\Omega_e)}\frac{c^2}{\omega^2L_n^2n_{cr}^2}-\frac{c^2n_{cr}^2}{\omega^2L_\theta^2}. \tag{22}$$

If the roots of the quadratic, Eq. (21) are a and b, and assuming that α is positive, we may write $k^2=\alpha(x-a)(x-b)$. The energy transmission coefficient T is given by $T=\exp(-2\kappa)$ where

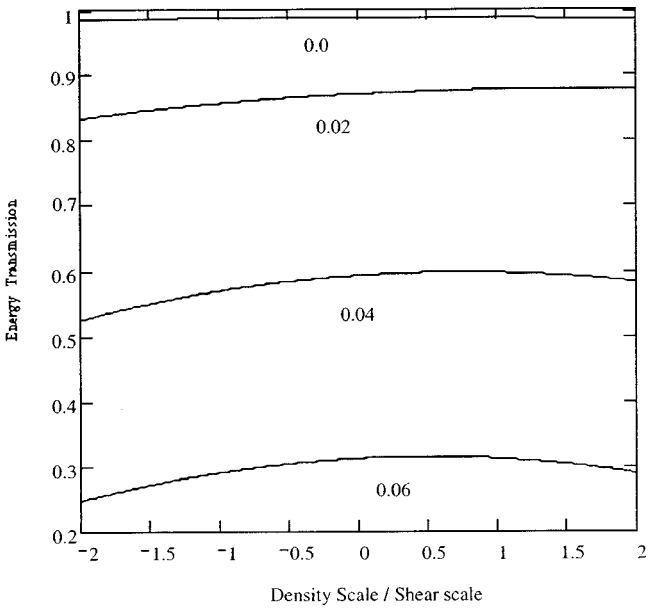

FIG. 3. Transmission coefficient for O-mode to X-mode conversion as a function of the shear parameter, r = density scale/shear scale, for various values of $\delta\equiv n_z-n_{cr}$. The curves are labeled by the corresponding value of δ. Frequency = 60 GHz, density scale length $L_n=0.1$ m, $n_y=0.01$.

$$\kappa=\alpha^{1/2}\int_a^b[(x-a)(x-b)]^{1/2}dx. \tag{23}$$

Using the result

$$\int_a^b[(x-a)(x-b)]^{1/2}dx=i\frac{\pi}{8}(a-b)^2, \tag{24}$$

and Eq. (22), we obtain

$$T=\exp\left[-\frac{\pi}{4}\left\{\frac{2\omega}{(\omega+\Omega_e)}\frac{1}{L_n^2n_{cr}^2}-\frac{n_{cr}^2}{L_\theta^2}\right\}^{1/2}\frac{c}{\omega}(a-b)^2\right]. \tag{25}$$

Substituting the explicit values of the roots a and b of Eq. (21), and introducing the ratio $r=L_n/L_\theta$, Eq. (25) becomes

$$T=\exp\left[-\pi\frac{L_n\omega}{c}\frac{\left(\frac{2\delta}{n_{cr}}-rn_yn_{cr}\right)^2+n_y^2\left\{\frac{2\omega}{(\omega+\Omega_e)}\frac{1}{n_{cr}^2}-r^2n_{cr}^2\right\}}{\left(\frac{2\omega}{(\omega+\Omega_e)}\frac{1}{n_{cr}^2}-r^2n_{cr}^2\right)^{3/2}}\right]. \tag{26}$$

For zero shear, $r=0$, the expression given in Eq. (26) is in agreement with Eq. (19) of Mjolhus for the case $\alpha=\pi/2$.

The behavior of the transmission coefficient for a 60 GHz source and conditions relevant to MAST is illustrated in Figs. 3–12. In these figures the transmission coefficient is plotted as a function of the parameter r for four values of the mismatch parameter δ. In Figs. 3–5 the density scale length $L_n=0.1$ m and n_y takes the values 0.01, 0.03, and 0.05, respectively. It is clear that the transmission coefficient is not very sensitive to the magnetic shear. It is, however, sensitive to the mismatch parameter δ and to the value of n_y. The transmission is reduced when $L_n=0.5$ m. This is shown in Figs. 6–8 where smaller values of δ were used and n_y runs from 0.01 to 0.03 between Figs. 6 and 8.

Downloaded 08 Aug 2012 to 194.81.223.66. Redistribution subject to AIP license or copyright; see http://pop.aip.org/about/rights_and_permissions

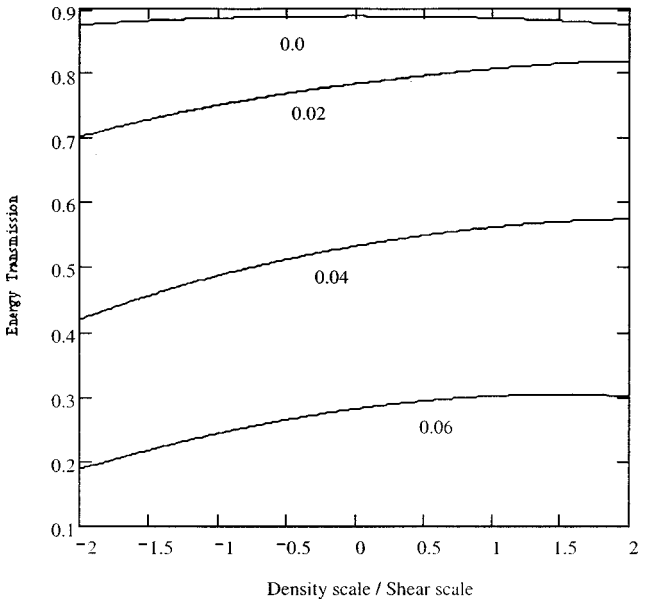

FIG. 4. Transmission coefficient as a a function of r for $n_y=0.03$ and same range of δ-values as Fig. 3.

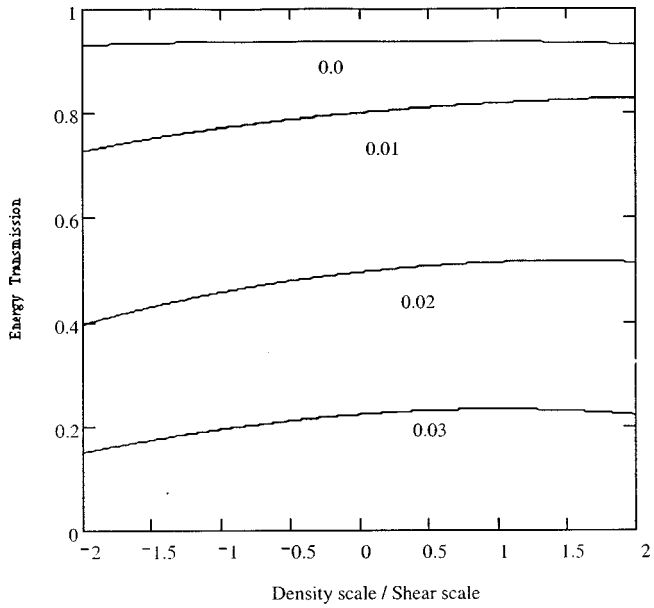

FIG. 6. Same as Fig. 3 except $L_n=0.5$ m.

While 60 GHz, which corresponds to the fourth harmonic on MAST, is a common frequency for gyrotron systems, it might be advantageous to use lower frequencies if a new system were being designed. For this reason, and for comparison, results are now presented for a frequency of 15 GHz corresponding to the fundamental frequency on MAST, close to the magnetic axis. These results are shown in Figs. 9 and 10. In Fig. 9, $L_n=0.1$ m and in Fig. 10, $L_n=0.5$ m. In both cases, $n_y=0.03$, but as before, smaller values of δ are used for the larger length scale. In this case, the transmission is more sensitive to the magnetic shear. Contour plots of the transmission are shown in Figs. 11 and 12 in which n_y varies between -0.1 and 0.1 along the x axis and δ varies between the same limits in the y direction. The frequency was taken to be close to the fundamental and $L_n=0.2$ m. The case without shear is shown in Fig. 11 whereas the parameter $r=1$ in Fig. 12. It can be seen that the main effect of shear is to tilt the diagram, but the size of the window through which significant transmission is obtained is not changed greatly.

III. THE DAMPING OF ELECTRON BERNSTEIN WAVES

Electron Bernstein waves are very short wavelength modes which are strongly damped near to a harmonic resonance. In order to quantify the absorption properties of electron Bernstein waves we have solved the full hot plasma, electromagnetic dispersion relation for waves propagating obliquely to a uniform magnetic field in a uniform plasma.

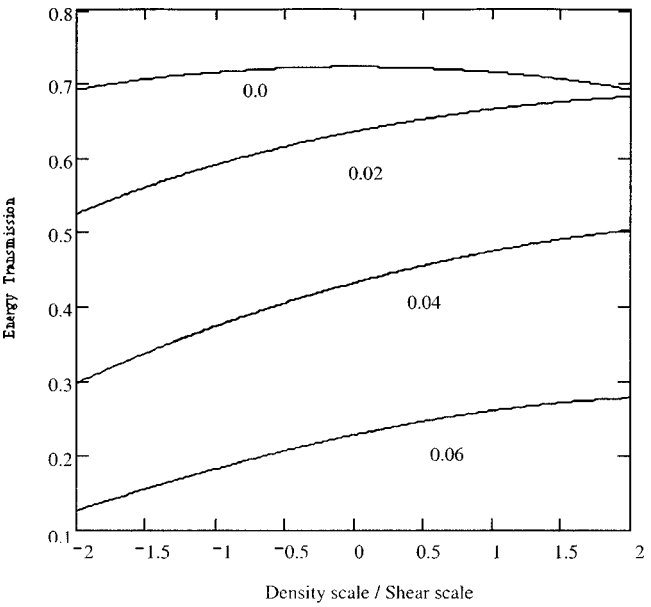

FIG. 5. Same as Figs. 3 and 4 but $n_y=0.05$.

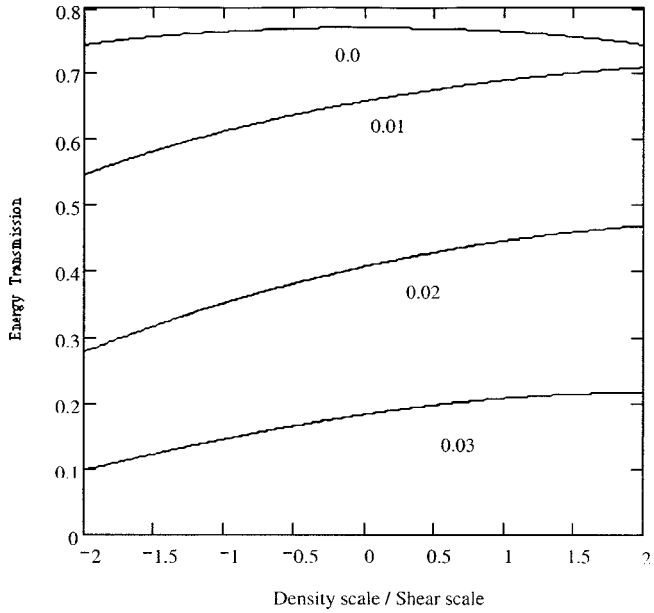

FIG. 7. Same as Fig. 3 except $n_y=0.02$ and $L_n=0.5$ m.

Downloaded 08 Aug 2012 to 194.81.223.66. Redistribution subject to AIP license or copyright; see http://pop.aip.org/about/rights_and_permissions

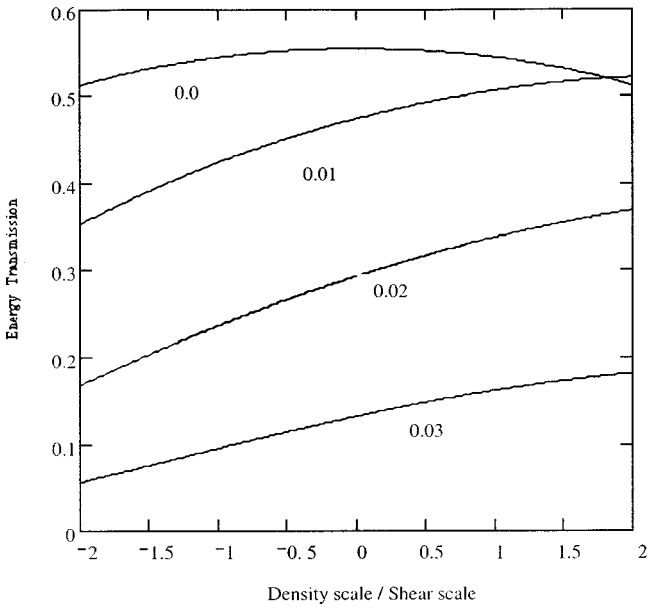

FIG. 8. Same as Fig. 3 except $n_y=0.03$, $L_n=0.5$ m.

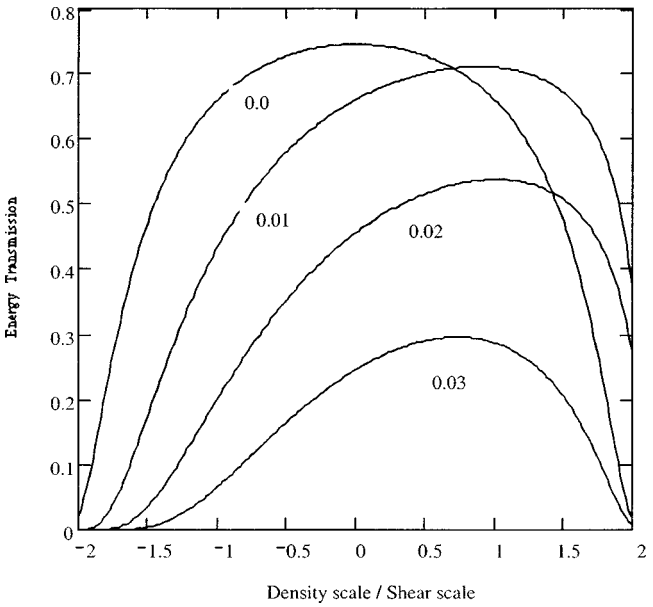

FIG. 10. Same as Fig. 3 except $n_y=0.03$, frequency = 15 GHz, $L_n=0.5$ m.

The dispersion relation is standard and is obtained, for example, from Stix.[5] We have used the nonrelativistic electron susceptibility tensor since we include a significant value of $k_\parallel$ and the absorption is due mainly to the Doppler shifted cyclotron resonance mechanism. The values chosen for $k_\parallel$ are guided by the value required for the O–X conversion process.

For a 60 GHz source on MAST the upper hybrid resonance can be chosen to lie between the fourth and fifth electron cyclotron harmonic resonances. The mode converted electron Bernstein wave will propagate from the upper hybrid resonance to the fourth harmonic resonance. Hence we apply the electron Bernstein wave root solver to a plane slab geometry in which the magnetic field varies as a function of x (the radial direction) but the density and temperature are assumed to be constant. The real and imaginary parts of the perpendicular refractive index, $n_\perp$, are calculated as a function of the parallel refractive index, $n_\parallel$, the ratio of the cyclotron frequency to the wave frequency and the ratio of the density to the O-mode cut-off density. The results for the region of the fourth harmonic are shown in Figs. 13–16. Figure 13(a) shows the variation of the electron cyclotron frequency divided by the wave frequency as a function of normalized distance. The ratio of the density (constant) to the O-mode cutoff density is shown in Fig. 13(b). The electron temperature, which is also independent of the spatial

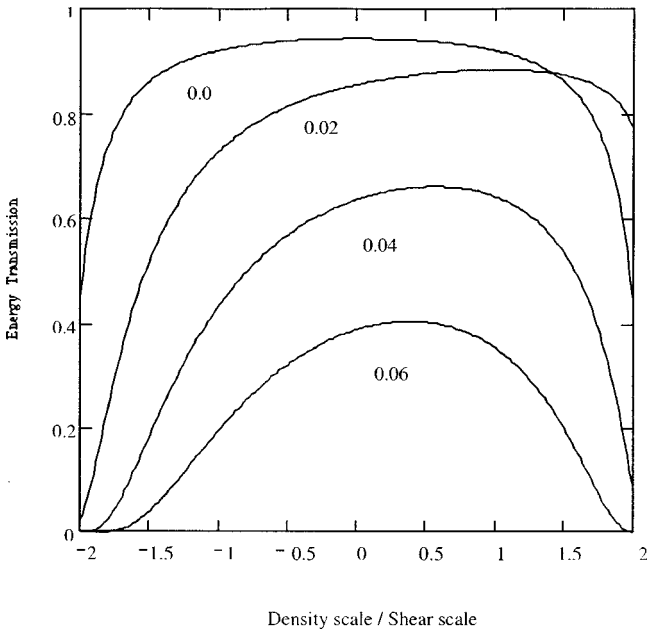

FIG. 9. Same as Fig. 4 except frequency = 15 GHz (fundamental resonance).

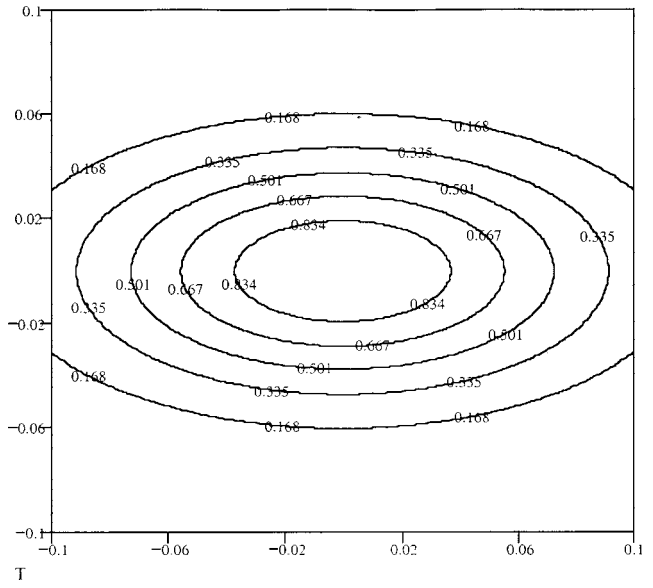

FIG. 11. Contour plots of the O–X transmission coefficient where the vertical axis is δ, and the horizontal axis is n_y (both axes vary between ± 0.1). Frequency = 15 GHz, $L_n=0.2$ m. This case refers to $r=0$, zero magnetic shear.

Downloaded 08 Aug 2012 to 194.81.223.66. Redistribution subject to AIP license or copyright; see http://pop.aip.org/about/rights_and_permissions

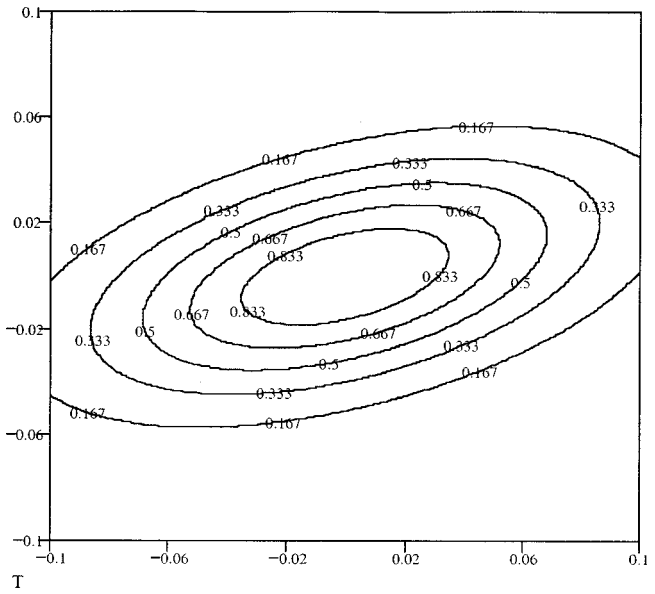

FIG. 12. Same as Fig. 11 except $r=1$.

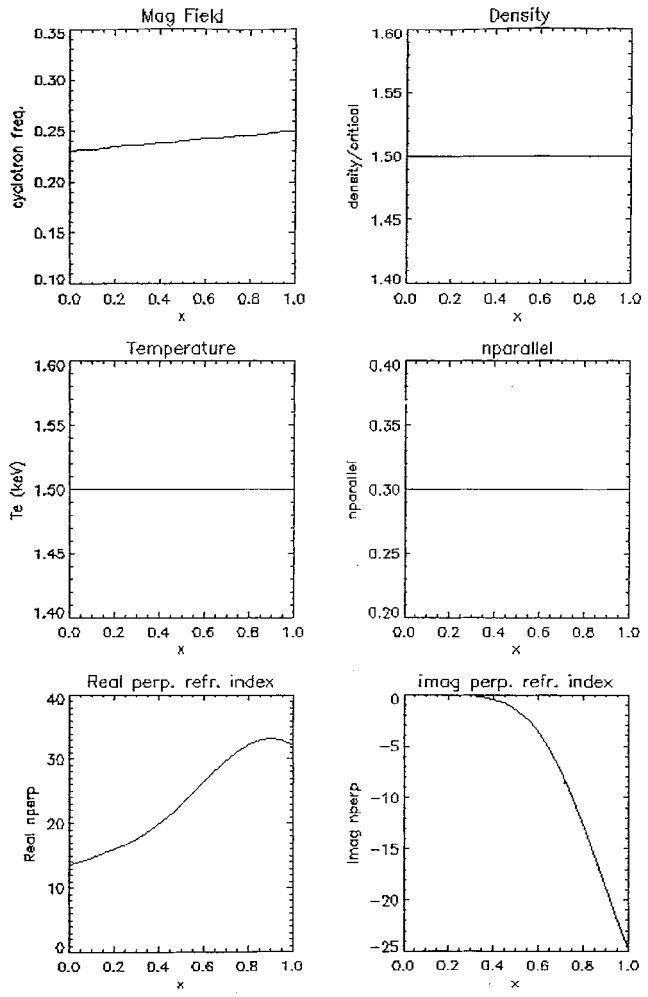

FIG. 13. Solution of local nonrelativistic hot plasma dispersion relation for the electron Bernstein wave root in the vicinity of the fourth harmonic (corresponds to 60 GHz on MAST) (a) variation of magnetic field shown through ratio $\Omega_e(x)/\omega_{\mathrm{RF}}$. (b) Density (constant) normalized to O-mode cut-off density, (c) electron temperature (constant) in keV, (d) parallel refractive index, $n_\parallel = ck_\parallel/\omega_{\mathrm{RF}}$ (e) real part of the perpendicular refractive index, $n_\perp$ as a function of the spatial variable, x, (f) imaginary part of the perpendicular refractive index, $n_\perp$ as a function of x.

variable, is given in Fig. 13(c), and Fig. 13(d) shows the value of $n_\parallel$. The real and imaginary parts of $n_\perp$ are given in Figs. 13(e) and 13(f). In Figs. 14–16 only the real and imaginary parts of $n_\perp$ are shown since the magnetic field, density and temperature are the same as in Fig. 13. The only change of parameter in Figs. 14–16 is that $n_\parallel$ takes the values 0.5, 0.7, and 0.9, respectively. The critical value of $n_\parallel$ for the O–X conversion is ~ 0.43. Using the parameters of MAST, we can translate the normalized units of Figs. 13–16 into physical values. Thus making use of the usual expression for the toroidal magnetic field, B_0R_0/R, with $B_0=0.63$ tesla and $R_0=0.7$ m, we note that one spatial unit in Fig. 13(a) corresponds to 0.071 m. For a frequency of 60 GHz the density corresponds to 6.75×10^{19} m^{-3}.

An approximate estimate of the strength of the damping can be obtained by using the plots of $\mathrm{Im}\, n_\perp$. Note that $\mathrm{Im}\, n_\perp < 0$, corresponding to the backward wave nature of the electron Bernstein wave. The absorption is given by $\exp(-\tau_n)$ where τ_n is the optical depth, $\tau_n = 2\int \mathrm{Im}\, k_\perp(x)dx$ and the subscript n refers to the particular harmonic. The magnitude of the optical depth corresponding to the fourth harmonic can be obtained graphically from Fig. 13(f) (say) by estimating the triangular area between the curve and the horizontal and vertical axes. Thus, for a frequency of 60 GHz we obtain $\tau_4 \approx 1400$. This is typical of all the cases that we have considered, both for $\omega \simeq 4\Omega_e$, $\omega \simeq \Omega_e$ and for higher densities. Such enormous optical depths mean that the electron Bernstein wave would be totally absorbed well before it reached the center of the resonance region. This, in turn, means that the absorbing electrons would be those with large values of velocity parallel to the equilibrium magnetic-field, $v_\parallel$, all with the same sign. This property of electron Bernstein waves makes them very good candidates for efficient current drive, both on and off axis.

IV. SUMMARY AND CONCLUSIONS

Since the O-mode and X-mode are not suitable for heating the high density, low magnetic-field discharges characteristic of spherical tokamaks, we have analyzed the prospects for electron Bernstein wave heating of these devices, and we have considered the case of MAST as a specific example. As MAST has ~1.5 MW of gyrotron power at 60 GHz available, we have used this frequency in a number of the calculations. However, since electron Bernstein waves do not have a density limit and are strongly damped at high harmonics as well as at the fundamental and low harmonics, these waves offer considerable flexibility in the choice of frequency. We have, therefore, also carried out calculations of excitation and absorption of electron Bernstein waves at the fundamental.

The principal problem faced by electron Bernstein wave heating is that of coupling an external source to these short wavelength electrostatic waves. The most promising mecha-

Downloaded 08 Aug 2012 to 194.81.223.66. Redistribution subject to AIP license or copyright; see http://pop.aip.org/about/rights_and_permissions

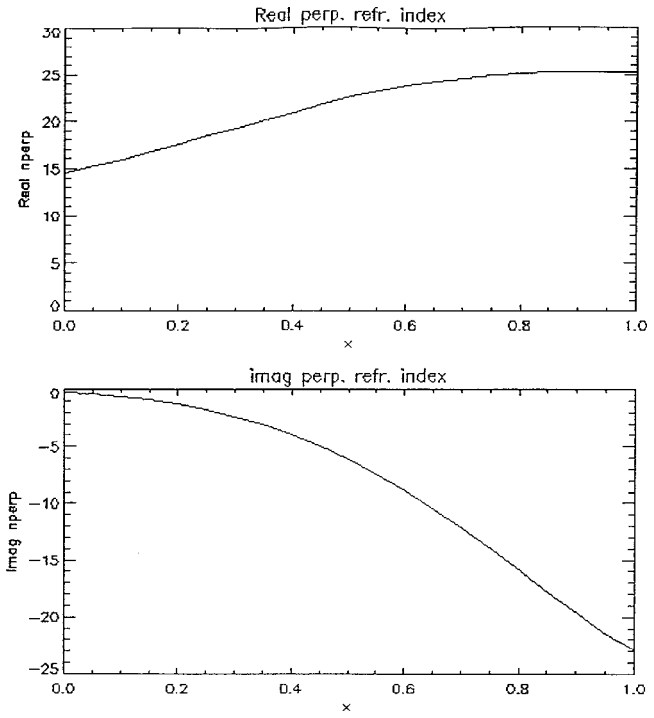

FIG. 14. Solutions of the local hot plasma dispersion relation for $n_{\|}=0.5$ (a) real part of $n_{\perp}$ (b) imaginary part of $n_{\perp}$.

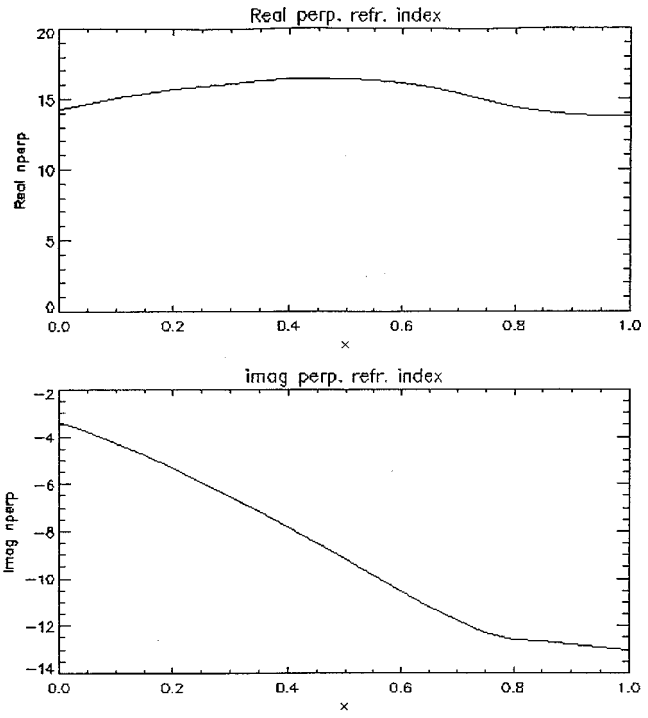

FIG. 16. Same as Fig. 14 except $n_{\|}=0.9$.

nism is through linear mode conversion at the upper hybrid resonance, for which there are two schemes. The first involves the tunneling of the X-mode through the evanescent region between the low density cutoff and the upper hybrid resonance, which has been analyzed in some detail in Refs. 4 and 6. In this paper we have concentrated on the second approach, first proposed for plasma heating in Ref. 8. The second approach involves the linear conversion of the O-mode to the X-mode at the O-mode cutoff where $\omega=\omega_{pe}$. For a critical value of $n_{\|}$ the high density X-mode cutoff coincides with the O-mode cutoff, resulting in a one hundred per cent transfer of the incident O-mode energy to the X-mode. The X-mode can then propagate unimpeded to the upper hybrid resonance and convert to the electron Bernstein wave as in the first case.

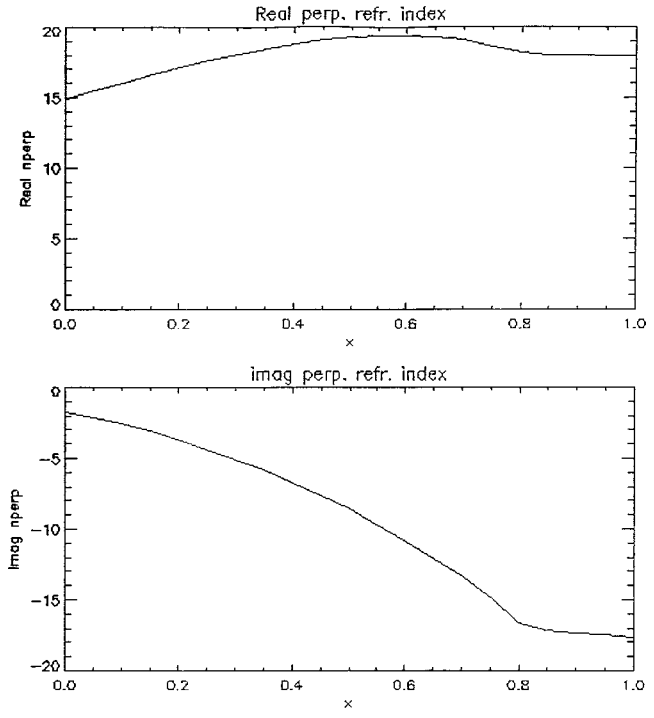

FIG. 15. Same as Fig. 14 except $n_{\|}=0.7$.

It is worth commenting that the two coupling schemes which rely on linear mode conversion are complementary in the following sense. In order for the X-mode to convert to the electron Bernstein wave at the upper hybrid resonance it must tunnel through the evanescent layer between the low-density cutoff and the resonance. On the other hand, for the O–X–EBW coupling scheme, the X-mode approaches the upper hybrid resonance from the higher density plasma resonance. In this case, total conversion of the X- mode to the electron Bernstein wave requires that there be no tunneling through the low density evanescent region. Since the tunneling properties of this region depend on its density gradient, the two schemes provide a certain flexibility of choice depending on the eventual profile.

Previous calculations of this process have been extended by including the effect of magnetic shear which can be very strong in spherical tokamaks. It was found that the size of the transmission window was hardly changed by the presence of magnetic shear.

In spherical tokamaks, the poloidal magnetic field can be comparable to or greater than the toroidal field in the outer regions of the plasma on the outboard side. For example, when the plasma current in MAST is of the order of or greater than 1 MA, the total magnetic field is nonmonotonic

Downloaded 08 Aug 2012 to 194.81.223.66. Redistribution subject to AIP license or copyright; see http://pop.aip.org/about/rights_and_permissions

in this region. This feature makes it possible for an electron Bernstein wave to be absorbed at a centrally located electron cyclotron harmonic resonance, e.g., $\omega \simeq 3\Omega_e$, without passing through another harmonic resonance in the outer regions.

A feature of the damping of electron Bernstein waves is the extremely large optical depths of the fundamental and harmonic resonances ($\tau_n \gtrsim 10^3$). This is extremely promising for current drive, both on- and off-axis, since it implies that the wave energy is absorbed in a small region on one side of the resonance, where the absorbing electrons would all have large values of the parallel velocity and would all be traveling in the same direction along the magnetic field.

In order to couple efficiently to electron Bernstein waves, as already demonstrated on the W7-AS stellarator,[9] it is necessary to design a high-frequency launch system which can be aligned very precisely with respect to the equilibrium magnetic field in order to achieve the required narrow spectrum of $n_\parallel$ incident on the critical surface. A diagnostic system designed to detect electron cyclotron emission produced by the inverse of the O-mode to X-mode to electron Bernstein wave conversion would be helpful in identifying the optimum launch conditions. A further important question concerns the evolution of $n_\parallel$ in a toroidal plasma since this determines the absorption region and the parallel velocities of the resonant electrons. Clearly, a toroidal ray tracing code is required to elucidate this question.

ACKNOWLEDGMENTS

We would like to thank Vladimir Shevchenko for helpful discussions and the referee for his constructive comments.

This work was partly funded by the United Kingdom Department of Trade and Industry and Euratom.

[1] A. C. Darke, M. Cox, J. R. Harbar *et al.*, *Proceedings of the 16th Symposium on Fusion Engineering, Piscataway, 1995* (Institute of Electrical and Electronics Engineers, Piscataway, NJ, 1995), p. 1456.
[2] A. Sykes and the START, NBI, MAST, and Theory Teams, Nucl. Fusion **39**, 1271 (1999).
[3] J. Spitzer, M. Ono, and M. Peng, Fusion Technol. **30**, 1337 (1996).
[4] A. K. Ram, *Proceedings of the 13th Topical Conference on Applications of RF Power to Plasmas, Annapolis, MD 1999* (American Institute of Physics, New York, 1999), p. 375.
[5] T. H. Stix, *Waves in Plasmas* (American Institute of Physics, New York, 1992), p. 11.
[6] A. Bers, A. K. Ram, and S. D. Schultz, *Proceedings 2nd Europhysics Topical Conference on Radio Frequency Heating and Current Drive of Fusion Devices, Brussels 1998*, edited by J. Jacquinot, G. Van Oost, and R. R. Weynants (European Physical Society, Petit-Lancy, 1998), p. 237.
[7] K. G. Budden, *The Propagation of Radio Waves* (Cambridge University Press, Cambridge, 1985), p. 532.
[8] J. Preinhaelter and V. Kopecký, J. Plasma Phys. **10**, 1 (1973).
[9] H. P. Laqua, V. Erckmann, H. J. Hartfuss, and H. Laqua, Phys. Rev. Lett. **78**, 3467 (1997).
[10] D. B. Batchelor and T. S. Bigelow, *Proceedings 12th Topical Conference on Radio Frequency Power in Plasmas, Savannah, 1997*, edited by P. M. Ryan and T. Intrator (American Institute of Physics, New York, 1997), p. 415.
[11] V. Shevchenko, ''ECE measurements via B/X/O mode conversion: A proposal to diagnose the q-profile in spherical tokamaks,'' Plasma Phys. Rep. (to be published).
[12] H. Weitzner and D. B. Batchelor, Phys. Fluids **22**, 1355 (1979).
[13] E. Mjolhus, J. Plasma Phys. **31**, 7 (1984).
[14] R. A. Cairns, *Radiofrequency Heating of Plasmas* (Adam Hilger, Bristol, 1991), p. 102.
[15] R. A. Cairns, *Radiofrequency Heating of Plasmas* (Adam Hilger, Bristol, 1991), p. 43.

Downloaded 08 Aug 2012 to 194.81.223.66. Redistribution subject to AIP license or copyright; see http://pop.aip.org/about/rights_and_permissions